

# Chapter 12

## Large Meteoroids as Global Infrasound Reference Events



Christoph Pilger, Lars Ceranna, Alexis Le Pichon and Peter Brown

**Abstract** The explosive fragmentation of large meteoroids entering the Earth's atmosphere is one of the strongest sources of infrasound and can be detected at distances of thousands of kilometers by arrays all over the world. Influence parameters on the detection capability are quantified for a single infrasound station and for the complete infrasound network of the International Monitoring System (IMS) operated by the Comprehensive Nuclear-Test-Ban Treaty Organization (CTBTO). They are applied to a number of strong bolides of the past 15 years including the 2013 Chelyabinsk, 2010 Sulawesi, and 2009 North Pacific events. Long-range infrasound propagation modeling and realistic atmospheric background conditions are used to identify propagation paths that connect the sources and globally distributed receivers, highlighting usual as well as unusual propagation pattern, to stations detecting and stations not detecting a meteorite event. Potential influences on infrasound detection capability are due to the directivity of the acoustic source energy emission, the long-range ducting via stratosphere and thermosphere and the diurnal change of meteorological parameters and noise conditions at the stations during the signal arrivals. Since infrasound of large bolides has probably the most similar characteristics to an atmospheric nuclear explosion, it can be utilized as reference event for studies on the global performance of the CTBTO infrasound network. Detections and non-detections of bolide infrasound at the more than 40 operational IMS infrasound stations are studied for the estimation of station and network performance and thus verification of nuclear test ban.

---

C. Pilger (✉) · L. Ceranna  
Federal Institute for Geosciences and Natural Resources (BGR),  
Hannover, Germany  
e-mail: christoph.pilger@bgr.de

A. Le Pichon  
CEA, DAM, DIF, F-91297 Arpajon, France

P. Brown  
Department of Physics and Astronomy, University of Western Ontario,  
London, ON, Canada

## 12.1 Introduction

The explosive fragmentation of large meteoroids entering the Earth's atmosphere is one of the strongest existing sources of infrasonic waves and can be detected by infrasound arrays all over the world. Pressure perturbations of the strongest bolide events were detected at distances of thousands of kilometers, while for the 2013 Chelyabinsk superbolide, arrivals at long orthodrome distances (above 20,000 km) and after complete circumnavigations of the globe (up to 87,000 km) were recorded. This event was quantified having an equivalent explosive yield of up to 500 kt of TNT, being the most energetic global reference event ever recorded by the infrasound component of the International Monitoring System (IMS) network operated by the Comprehensive Nuclear-Test-Ban Treaty Organization (CTBTO) (Marty 2019).

Influence parameters on the detection capability of a single infrasound station on the one hand and of the complete global IMS infrasound network on the other hand are investigated within this study and applied to a number of strong meteoroid events of the past 15 years. Long-range infrasound propagation modeling and realistic atmospheric background conditions are used to identify propagation paths that connect the sources and globally distributed receivers. Infrasound propagation modeling calculations are performed to all IMS stations, highlighting usual as well as unusual propagation pattern, to stations detecting and stations not detecting a meteoroid event. Potential influences on infrasound detection capability are due to the directivity of the acoustic source energy emission, the long-range ducting via stratosphere and thermosphere, and the diurnal change of meteorological parameters and noise conditions at the stations during the signal arrivals.

Since the explosive fragmentation of large bolides during their atmospheric entry generates infrasound that shows probably the most similar characteristics to an atmospheric nuclear explosion, having comparable yields and generating similar pressure signatures, it can be utilized as reference event for studies on the global performance of the CTBTO infrasound network. Detections and non-detections of meteoroid infrasound at the more than 40 operational IMS infrasound stations are studied for the estimation of station and network performance and thus verification of nuclear test ban.

## 12.2 Infrasound from Meteoroids

Meteoroids are fragments of comets, asteroids, and planetoids entering the Earth's atmosphere. During their descent toward the surface, they heat up, disintegrate, fragment, or explode at certain altitudes typically between 10 and 100 km. Some fragments may even reach the ground and leave impact craters and remaining material, so-called meteorites. The luminous effect of heating up and exploding in the atmosphere is called meteor or fireball, while the body entering the atmosphere is often called bolide or meteoroid. The term meteoroid is further used in this chapter to

describe the material as well as the event of entry and explosion, generating shockwaves detectable as infrasound in the atmosphere (Silber and Brown 2019).

Infrasound generated by meteoroids is either a product of the trajectory of the atmospheric entry or of the final fragmentation and explosion at the end of the trajectory, while infrasound from the impact of meteorite remnants on the surface is a tertiary negligible effect for this study. Depending on the origin of the infrasound, a line source characteristic can be assumed to be due to the extended cylindrical shape of the trajectory and a point source due to a spherical explosion at the point of fragmentation (see Ens et al. 2012; Silber and Brown 2014; Hennenon et al. 2015).

Infrasound from the line or point source origin propagates through the atmosphere and can be detected by infrasound arrays, as, e.g., the IMS infrasound stations distributed all over the globe. Comparable to an atmospheric nuclear or conventional explosion, the yield of the exploding meteor and generated shock wave can be quantified in kilotons of TNT equivalent ( $1 \text{ kt TNT} = 4.185 \times 10^{12} \text{ J}$ ). Empirical relations (e.g., Silber and Brown 2019) are used to estimate the kinetic energy of meteoroids entering the atmosphere and compare it to the explosive yields observed and quantified by remote sensing, optical observations, and pressure recordings. The frequency content of meteoroid infrasound detected at remote infrasound stations is mainly situated at frequencies below 1 Hz, since higher frequencies are attenuated after long-range propagation in the atmosphere. The stronger the yield of a meteoroid event, the lower is the dominant frequency containing most of the acoustic energy. Large bolides with tens to hundreds of kt TNT equivalents have dominant frequencies as low as 0.1–0.025 Hz (periods of 10–40 s).

One of the first meteoroid events scientifically investigated and recorded by early microbarometers (see Whipple 1930) is the Tunguska meteoroid of the 30 June 1908, where a large meteoroid exploded over Siberia at approximately 10 km altitude with a very strong yield estimated as high as 10–12.5 Mt TNT. Other strong meteorite events during the following decades were investigated by improved observation technology and their characteristics quantified by novel scientific approaches (see ReVelle 1997; Edwards 2010; Silber and Brown 2019 for an overview on the history and physics of meteor generated infrasound).

With the beginning of IMS infrasound operations and the construction of stations in a global network in the late 1990 and early 2000 years, the number of long-range and global scale detections of meteoroid events strongly increased and a number of prominent meteoroid events were detected by multiple IMS infrasound stations in the following years as well as documented in scientific literature. Table 12.1 lists a number of these events and some characteristics as reported in the corresponding literature (Brown et al. 2002; Arrowsmith et al. 2008; Silber et al. 2011; Arrowsmith et al. 2013; Le Pichon et al. 2013).

The extraordinary meteoroid of Chelyabinsk, Russia in 2013 was the strongest infrasound event recorded since the beginning of the IMS infrasound network operations and its yield was estimated with half a megaton TNT equivalent (Brown et al. 2013). Until that time, all prior detections of the IMS network were only investigated with respect to the direct, shortest line connection between the infrasonic source and the signal detecting array, the so-called short orthodrome.

**Table 12.1** Large meteoroid events recorded by multiple IMS stations

Event	Region	Yield (kt TNT equivalent)	Number of detecting IMS stations	Maximum observation distance (km)
25 Aug 2000	Western Pacific	3	3	5,925
23 Apr 2001	Western Pacific	1–10	4	9,526
03 Sep 2004	Antarctica	12	6	12,918
07 Oct 2004	Indian Ocean	10–20	6	17,241
09 Dec 2006	Egypt	10–20	6	11,629
08 Oct 2009	Sulawesi	31–50	17 (23 after reanalysis)	17,509
25 Dec 2010	North Pacific	33	12 (21 after reanalysis)	14,906
15 Feb 2013	Chelyabinsk	500	20 (32 total detections)	86,663

For the Chelyabinsk meteoroid, a systematic analysis was performed (Le Pichon et al. 2013) to also identify signatures traveling long orthodrome paths between source and receivers (at distances of 20,000–40,000 km) and those, which circumnavigated the globe once or twice and were still detected at certain infrasound stations. A total of 12 more detections between 20,000 and 87,000 km were identified.

Due to the fact that strong infrasound source signals can potentially travel longer distances than 20,000 km and still be detectable, the next strongest meteoroid events of the last years (Sulawesi 2009 and North Pacific 2010) are reanalyzed within this study and compared to Chelyabinsk results to identify further station detections, focusing on long-range propagation and global detections even along the long orthodrome.

### 12.3 The Chelyabinsk, Sulawesi, and North Pacific Meteoroid Events

The Chelyabinsk meteoroid descended and disintegrated over the Ural Mountains with meteorite fragments up to 650 kg reaching the surface near the Russian town of Chelyabinsk and the nearby lake Cherbakul. Astronomical observations (Borovička et al. 2013) identified the object as a small asteroid with an initial diameter of about 17–20 m and a mass of 10,000 tons. The visually observed trajectory was 254 km long with a westward azimuth direction and a shallow elevation angle. The absolute brightness estimated from video records peaked with

a value of  $-28$  mag. at approximately 30 km altitude (Brown et al. 2013), categorizing the event as a superbolide temporarily brighter than the sun. A shock wave of the atmospheric entry affected buildings, smashed windows, and was multiply eye-witnessed (Popova et al. 2013). Visual recordings, including movies, of the fireball entering the atmosphere, fragmenting and descending toward the surface were available shortly after the event. The event was recorded by various remote sensing techniques, as, e.g., optical observations by ground-based and satellite instruments, seismometers, and infrasound sensors (Heimann et al. 2013; Miller et al. 2013; Tauzin et al. 2013; Antolik et al. 2014; Krasnov et al. 2014; de Groot-Hedlin and Hedlin 2014).

In contrast to the large attention of worldwide media to this event, the Sulawesi and North Pacific meteoroid events happened with a relatively low level of media response and public interest. Thunder-like sounds and ground-shaking were reported for the Sulawesi event near the city of Bone, South Sulawesi, Indonesia and the event was also captured on amateur video (see Silber et al. 2011 and references therein), but apart from this no damage was reported; in the case of the North Pacific meteoroid, the event happened above the Pacific Ocean and far from the shore. Nevertheless, observations by remote sensing means and the infrasound detections of the IMS provided information about these two events and initiated further research with regard to these cases (Silber et al. 2011; Arrowsmith et al. 2013).

The Sulawesi meteoroid entered the atmosphere over an island region of Indonesia at a very steep elevation angle in a south-southwest to north-northeast direction. The height of maximum brightness and final fragmentation/explosion was 19.1 km, although prolonged fragmentation between 20 and 30 km altitude likely took place. The North Pacific meteoroid entered the atmosphere about 1500 km east of Japan with an initial mass of about 820 tons, diameter of 7.5–8 m, and a steep elevation angle in a northwest to southeast direction. Table 12.2 summarizes the characteristics of atmospheric entry for the three meteoroid events.

Figure 12.1 shows the global detections of the IMS infrasound network in short and long orthodrome distances from the Chelyabinsk, Sulawesi and North Pacific meteoroids for 2 days following each event. Chelyabinsk detections are shown as

**Table 12.2** Characteristics of the Sulawesi, North Pacific, and Chelyabinsk meteoroid events

	Sulawesi	North Pacific	Chelyabinsk
Explosion location	4.2°S, 120.6°E	38°N, 158°E	54.8°N, 61.1°E
Explosion altitude (km)	30	19.1	26
Time of entry (UTC)	08 Oct 2009, 02:57	25 Dec 2010, 23:24	15 Feb 2013, 03:20
Azimuth angle (°)	27.5	147.2	279.5
Elevation angle (°)	67.5	61	16.5
Speed (km/s)	19	22.1	18.5
Explosive yield (kt)	31–50	33	500

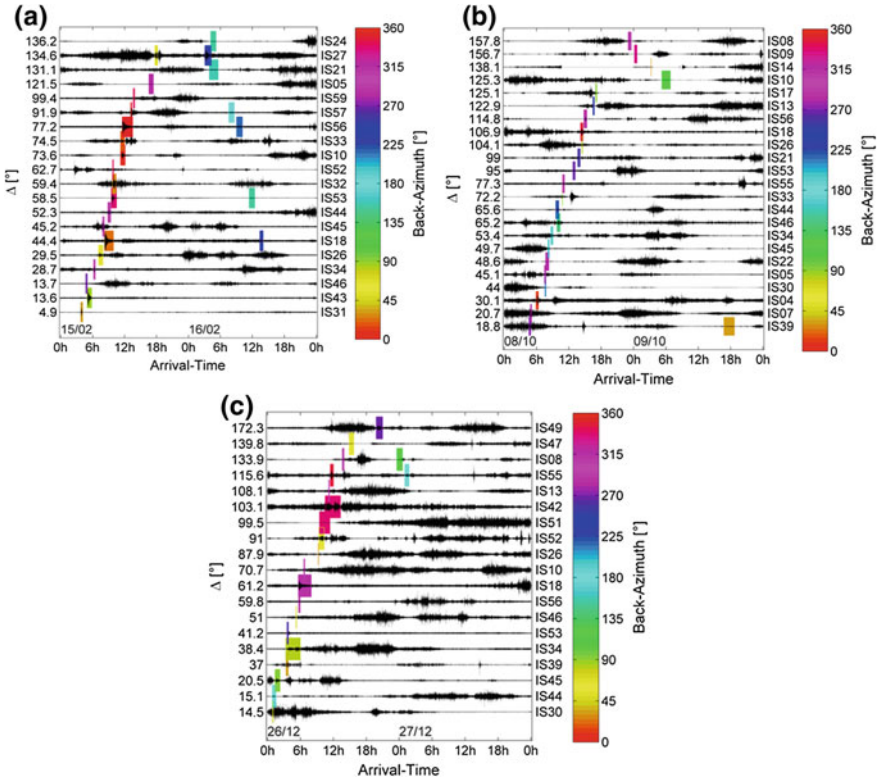


**Fig. 12.1** Barograms for 2 days following **a** the Chelyabinsk 2013, **b** the Sulawesi 2009 and **c** the North Pacific 2010 meteoroid event. Averaged phase-aligned recordings of the detecting IMS infrasound stations are shown using normalized amplitude. Arrival time is given in UTC, stations are sorted by propagation distance in degrees from the source (where 360° are one circumference of the Earth, 1° ≈ 110 km). Signals are band-pass filtered between 15 and 80 s. Detections of the short (0–180°) and long (180–360°) orthodrome arrivals are indicated by colored rectangles with corresponding signal duration and color-coded back azimuth

described in Le Pichon et al. (2013), while Sulawesi and North Pacific detections result from a very broadband PMCC reanalysis performed at the German NDC.

The reanalysis was performed using PMCC (Cansi 1995) version 4 with 23 frequency bands between 0.02 and 4 Hz, having the advantage of logarithmic scaled frequency stepping and an aligned window length from 500 to 30 s accounting for multiple cycles within each band.

In comparison to the number of already identified detections for the Sulawesi and North Pacific bolides described in literature (see Table 12.1), the reanalysis defined a higher number of detecting stations and total detections from the two

events. Furthermore, some long orthodrome ( $>20,000$  km) detections were identified for both events. One of the main goals of a complete reanalysis for these two events was to identify, if the Chelyabinsk meteoroid was a singular event generating such long-range infrasound that was also detectable on global scales or if other events were also strong enough to generate similar long-range signatures. No further signals were identified that circumnavigated the globe completely and were still detectable afterwards, but a number of detections between 20,000 and 40,000 km were identified for each event, increasing the range of interest for PMCC analyses, propagation modeling and global detection capability to the long orthodrome.

Two additional short orthodrome detections and five more long orthodrome detections were identified for the Sulawesi meteoroid using the PMCC reanalysis. Most long orthodrome detections were situated in South America, antipodal to the source region. This and a potential detection at I39PW (Palau) are indicative of a focusing effect of acoustic energy near the antipode and source regions. For the North Pacific meteoroid, six short orthodrome and three long orthodrome detection were identified complementary to the prior registered station observations. Two of the long orthodrome detections are also located near the antipodal point supportive of a focusing effect.

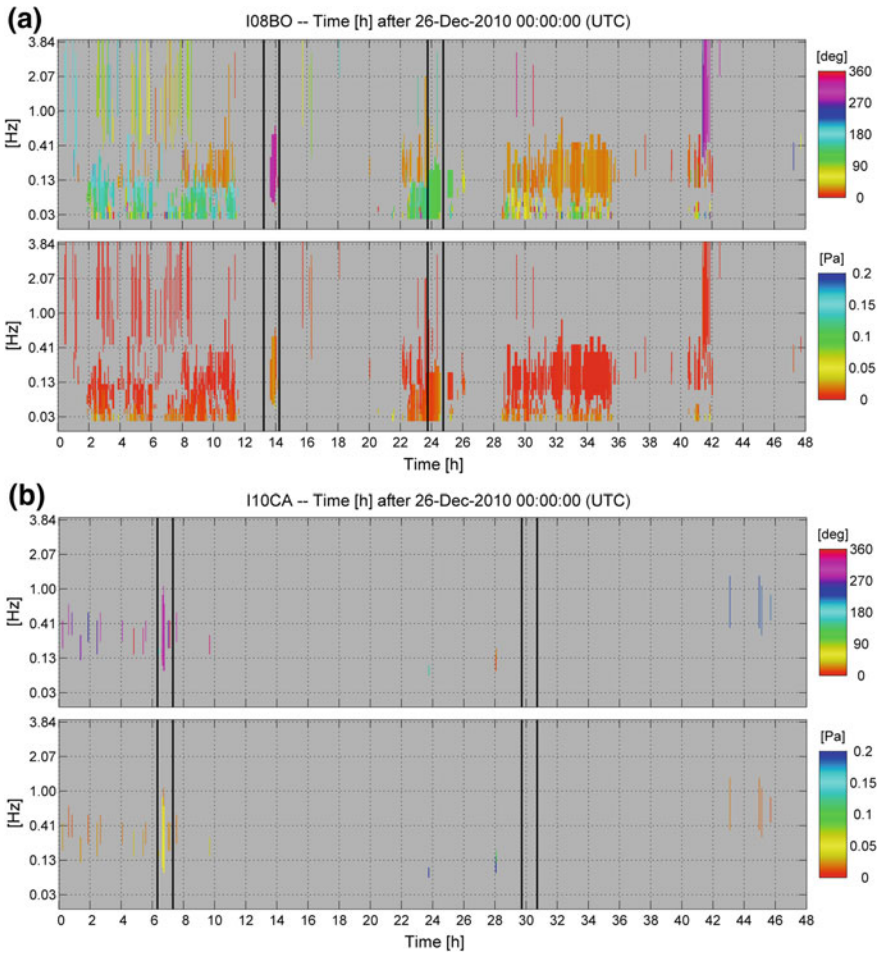
Since Sulawesi and North Pacific meteoroids were quite similar in source yield, region of origin, and resulting detections, only detections of the North Pacific event will be highlighted in the following.

Figure 12.2 shows PMCC analyses for North Pacific meteoroid detections at IMS infrasound stations I08BO (Bolivia), I10CA (Canada), I26DE (Germany), and I55US (United States). All four stations detected the meteoroid event along the short orthodrome (in  $307^\circ$ ,  $306^\circ$ ,  $27^\circ$  and  $352^\circ$  back azimuth directions, respectively), three of these detections were also reported in the CTBTO reviewed event bulletin, the I26DE detection was identified during the reanalysis in the low-frequency bands with a short but distinct signature associated to the meteoroid.

Additionally, the stations I08BO (Fig. 12.2a) and I55US (Fig. 12.2d) detected potential long orthodrome signatures from the North Pacific event, which correspond to the event in back azimuth directions ( $127^\circ$  and  $172^\circ$ , respectively) and estimated arrival times and show coherent signatures of low frequency, increased amplitude, and prolonged time duration. Other stations like I10CA (Fig. 12.2b) and I26DE (Fig. 12.2c) showed no long orthodrome signatures of the event. Potential reasons for this will be discussed in the following sections.

## 12.4 Infrasound Propagation Modeling

The modeling of infrasound propagation in the atmosphere can be performed using ray-tracing methods (e.g., Garcés et al. 1998; Drob et al. 2003, 2010; Pilger et al. 2013), even though this method is a high-frequency approximation applied here to low-frequency infrasound from large bolides. Within this study, a two-dimensional



**Fig. 12.2** PMCC analyses for 2 days following the North Pacific meteoroid event at **a** I08BO, **b** I10CA and **c** I26DE and **d** I55US. Color-coded information shows back azimuth directions in degree (upper frames) and amplitude in Pa (lower frames), frequencies range from 0.02 to 4 Hz (y-axes) and time ranges from 0 to 48 h following 26-Dec-2010, 00:00 UTC (x-axes). Vertical black bars frame 1 h windows of estimated signal arrival time using propagation modeling. Theoretical back azimuths expected for the meteoroid source in these frames are **a**  $307^\circ$  and  $127^\circ$ , **b**  $306^\circ$  and  $126^\circ$ , **c**  $27^\circ$  and  $207^\circ$ , **d**  $352^\circ$  and  $172^\circ$ . See text for further details

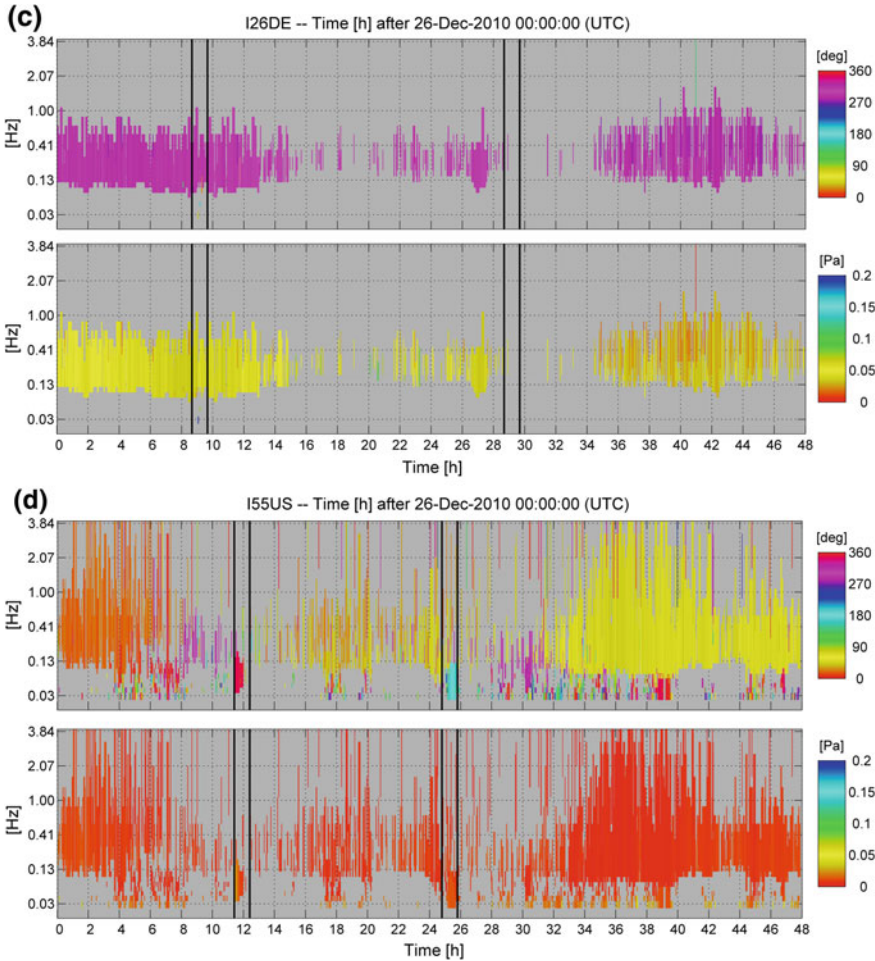


**Fig. 12.2** (continued)

finite differences ray tracer is used, which is part of the Consortium for Research in Elastic Wave Exploration Seismology (CREWES) software package (see <http://www.crewes.org/Reports/2000/2000-09.pdf> written by Margrave).

Background atmospheric conditions within this study are modeled using temperature and wind profiles from global ECMWF-91 ([www.ecmwf.int](http://www.ecmwf.int)) reanalysis data with a horizontal resolution of  $0.5^\circ$ , merged at the top of the model (0.01 hPa) with MSISE-00 and HWM-07 climatologies (Picone et al. 2002; Drob et al. 2008) in order to extend the profiles into the thermosphere. Wind and temperature profiles are interpolated over a spatial grid of  $200\text{ m} \times 200\text{ m}$  resolution in range and altitude, respectively, as a prerequisite for ray tracing with the same resolution.

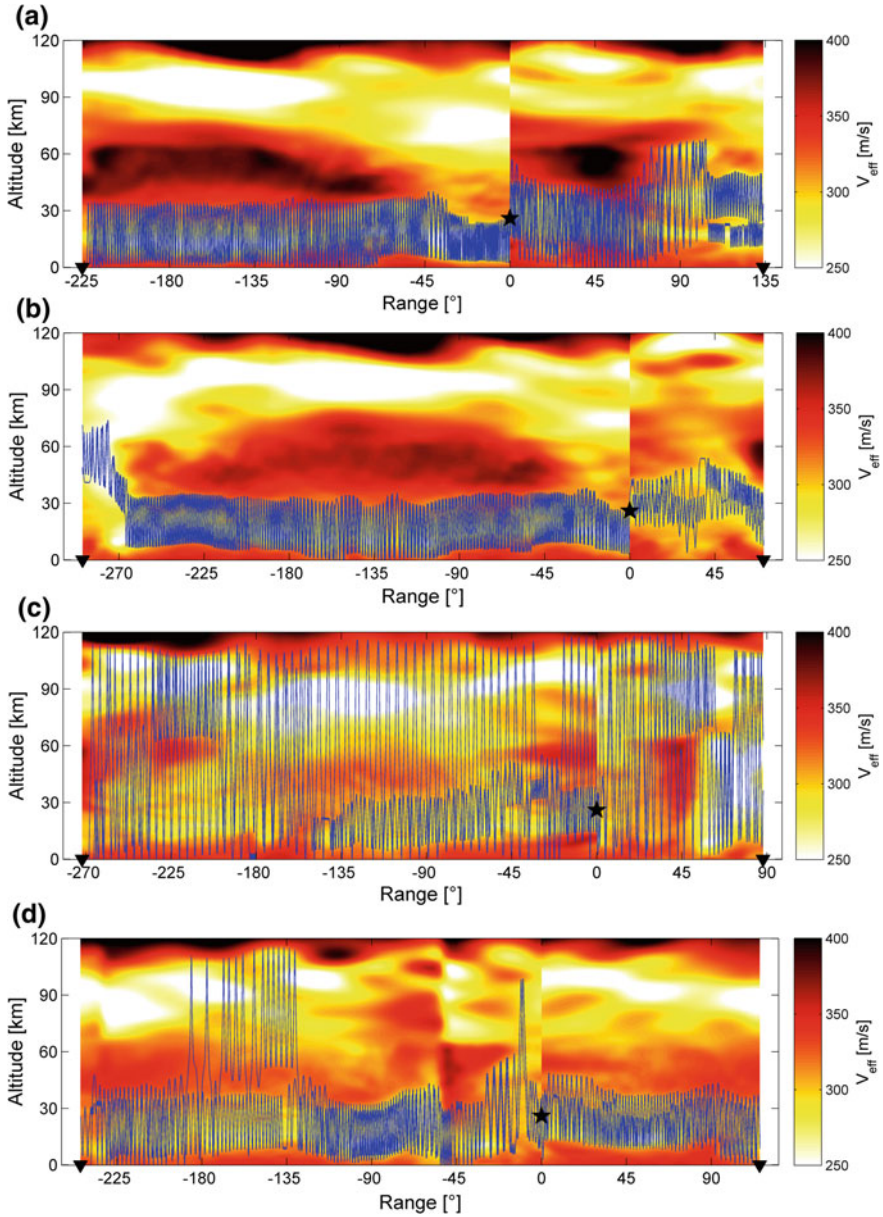


**Fig. 12.3** Propagation paths from the main explosion source of the North Pacific meteoroid at 26 km altitude to stations **a** i08BO, **b** i10CA **c** i26DE and **d** i55US using a two-dimensional finite differences ray tracer. Range-dependent atmospheric specifications are given by the ECMWF-91 model on 26 December 2010 at 06:00 UTC. The effective sound speed is color-coded, where values larger than the sound speed at the ground level (darker color) indicate altitudes of minimum ray turning height. The blast source is indicated by the black star and the receiving stations by black triangles, propagation distance is given in degree from the source. Short orthodrome propagation is shown to the right, long orthodrome propagation to the left

From temperature and wind values, the effective sound speed is derived for all source-to-station propagation directions along short and long orthodromes.

Results of the modeling for the Chelyabinsk meteoroid are described and depicted in Le Pichon et al. (2013). Apart from prevalent short orthodrome modeling of source–receiver paths, also long orthodrome ray paths, and complete circumnavigations of the globe are described. The propagation from the Chelyabinsk source location to, e.g., IMS infrasound stations I21FR (Marquesas Islands, South Pacific) and I27DE (Antarctica) is modeled and displayed in short and long orthodrome stratospheric ducts, simultaneously. For both stations, the ducting conditions are more stable along the long orthodrome and these detections have a higher amplitude even though traveling a larger distance compared to short orthodrome propagation. I21FR detected the event only along the long orthodrome. The propagation to I26DE (Germany) also includes large portions of thermospheric ducting for the short orthodrome (Ig1) and a further detection after a complete circumnavigation of the globe (Ig3). Multiple circumnavigations of the globe and subsequent detections at stations as, e.g., I18DK (Greenland) and I53US (Alaska) after a maximum propagation distance of 87,000 km were also documented and reported in Le Pichon et al. (2013).

For the Sulawesi and North Pacific bolides no detections after complete circumnavigations of the globe were registered, but the reanalysis using PMCC version 4 revealed some cases of long orthodrome detections previously unnoticed. Corresponding propagation modeling defined the theoretic arrival times for these detections which were, in general, good agreement to the observations.

Figure 12.3 shows four source-to-station propagation cases for the North Pacific meteoroid event, corresponding to the stations selected in Fig. 12.2a–d, with the modeling runs along the short and long orthodrome performed simultaneously.

For I08BO (Fig. 12.3a) and I55US (Fig. 12.3d), the propagation mostly takes place in stratospheric wave ducts and corresponds well to the station detections (Fig. 12.2a, d) along both orthodromes. Segments of elevated ducting and some reflections at thermospheric altitudes seem to have no negative effects on detectability in these cases.

For I10CA (Fig. 12.3b), the short orthodrome propagation shows elevated stratospheric ducting, but the lower reflection height returns near the station to altitudes below 10 km, which is in the order of the estimated infrasound wavelength and therefore low enough to permit a station detection corresponding to Fig. 12.2b. The signals following the long orthodrome path were not detected at this station, which might be due to the elevated ducting in the end of the propagation to altitudes of 40 km and above, which is a multiple of the infrasound wavelength and probably too high for any detection. Noise conditions at the station and the large distance could furthermore be a reason for this long orthodrome non-detection.

For I26DE (Fig. 12.3c), the short orthodrome propagation only allows thermospheric ray paths to connect the source with the station. Although thermospheric propagation takes place over a large distance of 90° (10,000 km), a short orthodrome detection of the North Pacific meteoroid was identified at I26DE (see the previous section) which corresponds to the modeled thermospheric propagation. No

long orthodrome detection was identified at I26DE, which is well in agreement with no clear stratospheric duct along the long orthodrome, but only thermospheric or mixed thermo/stratospheric ray paths over a total distance of 30,000 km, which might prohibit such a long-range detection.

## 12.5 Global Detectability

Events like the 2013 Chelyabinsk meteoroid are strong enough to generate infrasound that is in principle detectable for each IMS infrasound station around the globe, since signals from the event were detected up to (and beyond) the maximum distance of 20,000 km to any station of the global network. Nevertheless, effects like source-to-station ducting and ambient noise conditions might be favorable or unfavorable for individual stations and permit or prohibit signal detection from case to case.

Pilger et al. (2015) investigated influence parameters for the detection capability of the IMS infrasound stations with respect to the Chelyabinsk meteoroid event, taking into account short and long orthodrome propagation. Influence parameters identified within this study are the effective sound speed ratio governing stratospheric ducting, the directivity of the meteoroid source (assuming line source emission effects), and the diurnal change of ambient noise conditions.

Propagation conditions from the source to a receiving station are favorable when a stratospheric duct is established (see Fig. 12.3 and corresponding text) and the performance of this propagation can be expressed and quantified using the effective sound speed ratio between stratosphere and surface (see Le Pichon et al. 2012).

As soon as the source signal is no longer considered a point source, but the potential effects of a line source (the fireball trajectory entering the atmosphere) are also taken into account, the signal energy distribution is no longer uniform in all directions, but azimuth-dependent, favoring perpendicular directions with higher acoustic energy emission over parallel ones (e.g., see ReVelle et al. 2004; Edwards 2010).

The strongest influences on the detection capability identified and quantified in Pilger et al. (2015) were due to the noise conditions associated with diurnal changes of stability and turbulence in the surface-near atmospheric boundary layer. For a synoptic view of all worldwide locations, independent of single station locations with their individual characteristics, a global average of the station noise background differences between night and day was derived and integrated in the detection capability estimations as a simplified day-to-night change value.

A summation of the three aforementioned effects and relative quantification for a global synoptic view of the intensity effects influencing the global detection capability can be given by the following formula (Pilger et al. 2015):

$$Q_{synoptic} = 0.5 \cdot Q_{ducting} + Q_{directivity} + \mu \cdot Q_{daytime} \quad [dB]$$

To derive  $Q_{synoptic}$  as dB quantified intensity ratio, effects from  $Q_{ducting}$  for amplitude reduction due to propagation,  $Q_{directivity}$  for the azimuth dependence and  $Q_{daytime}$  for the diurnal change of noise conditions are summed. The effect of  $Q_{ducting}$  is multiplied by 0.5 to convert from amplitude to energy ratio and the effect of a global all-station mean noise value  $Q_{daytime}$  is multiplied by  $\mu$  having values of 0 during nighttime and 1 during daytime. All  $Q$  values are negative, whereas ideal conditions are given by zero. See Pilger et al. (2015) for further details on the estimation and quantification of the different  $Q$  values.

Figure 12.4 shows a synoptic view of the influence parameters using a dB scale relative to ideal detection conditions (mean nighttime noise levels, perpendicular directions, and stratospheric ducting with high effective sound speed ratio).

It can be clearly observed from the synoptic view that the prerequisites for detection of the fireball event were favorable in Eastern Asia, North America, Greenland, Antarctica, and the Pacific Ocean while disadvantageous in Europe, Western Africa, South America, and the Atlantic Ocean. This distribution very well explains most of the short orthodrome detections and non-detections and many of the long orthodrome ones. The North America and Greenland region is especially favored by a synergy of the investigated influence conditions to also permit the observed Ig3 and Ig5 detections, while non-detections strongly cluster in the darker colored regions below the mean expectation value (contour line in Fig. 12.4).

To compare the Chelyabinsk meteoroid event with the other meteoroid test cases and investigate the general applicability of the derived influence parameters, synoptic views are also generated for the Sulawesi and North Pacific events in the same style as Fig. 12.4. Both events are similar in their nature, intensity, source region, and resulting detectability so only the North Pacific event is presented and further discussed here.

The influence of ducting and the corresponding effect of sound attenuation is quantified in the same manner as for Chelyabinsk meteoroid following Le Pichon et al. (2012). A central signal frequency of 0.1 Hz is chosen to derive the frequency-dependent decrease in signal amplitude due to long-range propagation depending on the effective sound speed ratio. Quantifying this effect results in a higher influence of ducting compared to its negligible influence in the Chelyabinsk case. This is due to the higher signal frequency chosen and the lesser total effect of the other influence parameters detailed hereafter.

Considering the influence of directivity, not only the azimuth direction of the atmospheric entry has to be taken into account for the Sulawesi and North Pacific meteoroids, but also the elevation angle. In contrast to the Chelyabinsk meteoroid case with a shallow entry angle of  $16.5^\circ$  and a long trajectory line within the atmosphere, Sulawesi and North Pacific have very steep entries (with  $60\text{--}70^\circ$  elevation angles) and correspondingly much shorter trajectories and line source effects on the acoustic energy emission. Quantifying the steepness effect with a cosine weighting function (where for Chelyabinsk the effect is already included in



Fig. 12.4 but resulting in negligible changes since  $\cos 16.5^\circ \approx 1$ ), the North Pacific meteoroid steepness reduces the overall directivity effect by a factor of 2 ( $\cos 61^\circ \approx 0.5$ ). Favorable azimuth directions for most acoustic energy emission in this case are Southwest and Northeast (directions toward Japan and Northern America), while Southeastern and Northwestern directions are unfavorable since they are parallel to the trajectory.

The influence of the diurnal change was quantified only having two-thirds of the effect as in the Chelyabinsk case; a global all-station mean value of the noise intensity increase during daytime was derived investigating power spectra of all stations, which resulted in a 4.2 dB (intensity) noise increase during daytime for the North Pacific case compared to 6.5 dB (intensity) in the Chelyabinsk case (see Pilger et al. 2015 for the method used). For the moment, only a station derived mean value is used to distinguish day and nighttime effects on the ambient noise level and thus detection capability of a station, a more sophisticated approach using, e.g., the global distribution of a meteorological parameter like boundary layer height as a direct proxy for expected noise influences is currently under investigation.

In general, the effects of directivity and diurnal noise changes are weaker than in the Chelyabinsk case, while ducting influences are increased. Figure 12.5 summarizes the three effects of ducting, directivity and daytime for the North Pacific meteoroid event in a synoptic view of the same style as in Fig. 12.4.

Regions favorable for detection as derived from this synoptic view are along the short orthodrome (Ig1): Japan, Northern America, Greenland, most of the Arctic and Antarctic Region, Australia, Southern Africa, and the Indian Ocean. Observations agree with this for Japan, Northern America, Greenland, and Antarctica, but only 2 of 10 available stations between Southern Africa and Australia performed detections. On the other hand, 5 of 7 available stations in the Eurasian continent made detections although being in regions unfavorable for detections. Disagreements might be explained by increased ambient noise conditions for many of the Southern hemisphere island and shore locations and by relatively short distances and thus higher signal amplitudes at Northern Hemisphere stations even in thermospheric propagation directions (e.g., see Fig. 12.3c, station I26DE) and during noisier daytime conditions.

For the long orthodrome (Ig2), Southern America, the South Pacific Region, Antarctica, and Eastern Asia are in a favorable position for detections. This fairly well agrees with long orthodrome detections in IS08, Bolivia and IS55, Antarctica but is necessarily limited in completeness since only 3 of 41 stations have identified long orthodrome detections.

Another observation that can be made when comparing Figs. 12.4 and 12.5 is that the total content of intensity loss (in dB) is higher in the Chelyabinsk case than in the North Pacific case, they are about 1 dB higher in a global mean and about 1.5 dB for an all-station mean. Especially the contoured regions with high negative (red) dB values, which are unfavorable for detections, are more pronounced in the

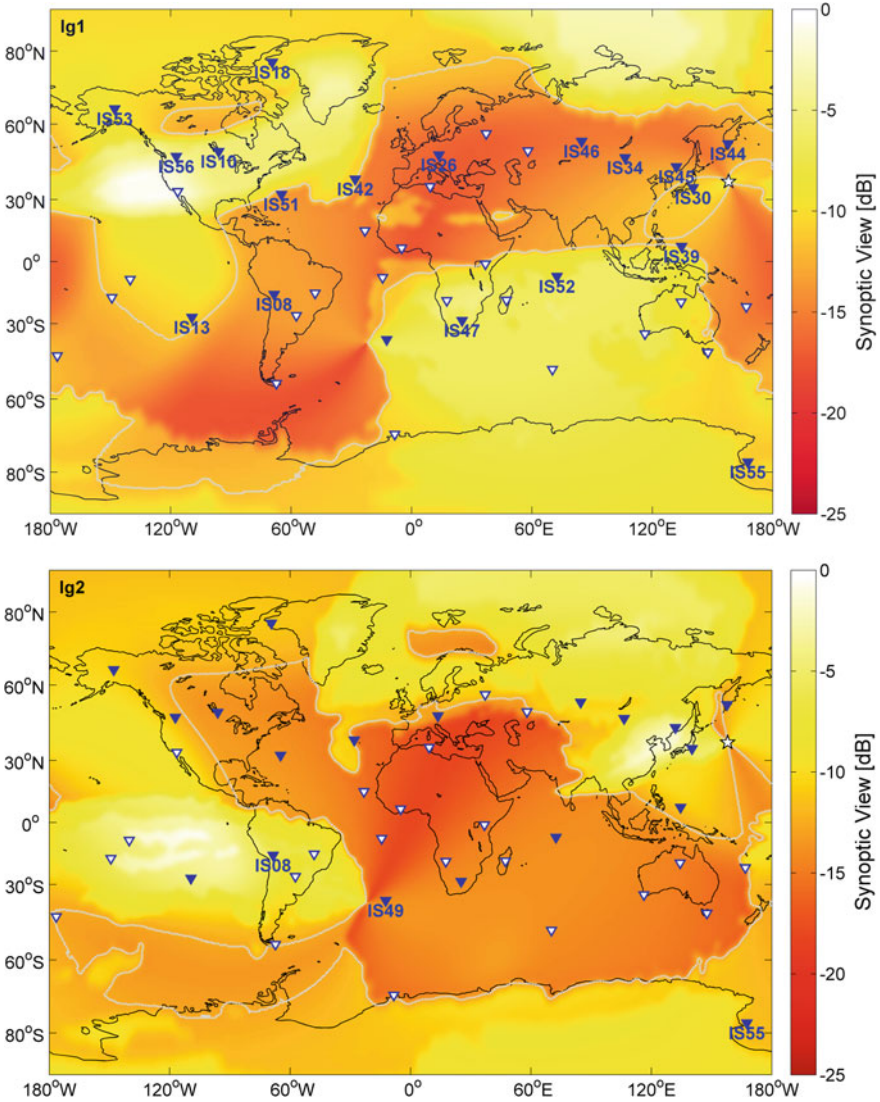


**Fig. 12.5** Synoptic view for the North Pacific meteoroid event in the same style as Fig. 12.4. The contour line shows the all-station mean value at  $-11.5$  dB

Chelyabinsk case and smoother in the North Pacific case. This well corresponds to a stronger effect of the influence parameters, especially directivity and diurnal noise changes, on detection capability in the Chelyabinsk case. Regions favorable or unfavorable for detections are strongly delimited from each other and observations very well fit this pattern, whereas for the North Pacific case, the boundary between

both regions is much smoother and many stations have observation although in unfavorable regions and vice versa. Detection capability parameters derived for the Chelyabinsk meteoroid event can thus only to a certain degree be applied to other strong meteoroid events.

## 12.6 Conclusions on Global Reference Events

Pilger et al. (2015) identified and quantified parameters that influence the detection capability of infrasound at global distances for the 2013 Chelyabinsk meteoroid as reference event. The parameters in the order from most to least influence were diurnal noise variation, line source directivity, and infrasound ducting.

Comparisons to other large meteoroid events of the last years in the course of this study revealed that the order and importance of the abovementioned influence parameters can change for other meteoroid events and that further specifications of these factors should be taken into account as well. These include not only the trajectories azimuth angle for directivity calculations but also the elevation angle, where a steeper entry angle into the atmosphere reduces the trajectory length and thus the influence of this parameter on detection capability.

Furthermore, the influence of diurnal changes of the ambient noise conditions could not only be estimated by a global or station-dependent mean value, but by a globally available time-dependent proxy, probably a meteorological value like the boundary layer height. To apply this parameter, further investigations on the latitude-dependent influence of the boundary layer on the ambient station noise are needed and other effects like station parameters as well as temperature and wind conditions also have to be taken into account.

In the context of ducting influences on detection capability, studies by Le Pichon et al. (2009, 2012) provide quantifications of the attenuation and signal amplitude reduction during stratospheric propagation and thus detection and location capability of the global IMS network (Ceranna et al. 2019). The propagation modeling performed for the Chelyabinsk and North Pacific meteoroid events moreover showed that also thermospheric propagation and arrivals (e.g., at I26DE) can be expected and this propagation component should be taken into account for ducting influence quantifications as well.

Investigations for the Chelyabinsk meteoroid showed that the ambient noise conditions and their diurnal changes have the strongest effect on detectability, whereas directivity had next strongest influences but was nearly independent of the elevation angle, since it was a very shallow entry into the atmosphere. Ducting effects were nearly negligible due to very low signal frequencies and thus attenuation values.

In contrast, for the North Pacific (and similarly the Sulawesi) meteoroid, directivity effects were reduced due to very steep entry angles and diurnal changes of the ambient noise conditions also had reduced global influence values, thus leaving ducting as a much stronger influence parameter.

It is concluded that the Chelyabinsk event on the one hand was a singular event with extraordinary strong yield and thus large acoustic energy emission over very long distances with very low signal frequencies, which resulted in a detection capability quite independent of propagation and attenuation, while on the other hand the classical estimation of detection capability relying on ducting and damping effects better suits for the other meteoroid events. These events also have yield estimates of more than one order of magnitude less compared to the Chelyabinsk case, which makes the 2013 Chelyabinsk meteoroid quite a unique infrasound source providing unprecedented insights in quantifying global infrasound detectability even at long orthodrome distances.

Studies provided here identifying influence parameters and generating synoptic views (Figs. 12.4 and 12.5) only take into account the comparison of relative values (day vs. night, perpendicular vs. parallel, high vs. low effective sound speed ratios) and cannot reflect absolute values as, e.g., the amplitudes observed at certain stations. To incorporate absolute values and directly compare them to observations, more sophisticated source models, improved propagation and distance effects, individual station performances including ambient noise models and technical specifications as well as global high-resolution specifications of meteorological background conditions have to be taken into account.

Studies on strong meteoroid events generally allow allocatable observations to be compared to model quantifications and thus support the investigation of potential influence parameters and estimation of new approaches to demonstrate the usefulness of meteorites as global reference events for CTBT (atmospheric) explosion monitoring and verification purposes.

The study of meteoroids as global infrasound reference events provided new insights to global infrasound detection capability and network performance, also supporting “lessons learnt from a comprehensive and global infrasound monitoring” (Le Pichon et al. 2019).

## References

- Antolik M, Ichinose G, Creasey J, Clauter D (2014) Seismic and infrasonic analysis of the major bolide event of 15 February 2013. *Seismol Res Lett* 85(2):334–343. <https://doi.org/10.1785/0220130061>
- Arrowsmith SJ, Re Velle DO, Edwards W, Brown PG (2008) Global detection of infrasonic signals from three large bolides. *Earth Moon Planet* 102:357–363. <https://doi.org/10.1007/s11038-007-9205-z>
- Arrowsmith SJ, Marcillo O, Drob DP (2013) A framework for estimating stratospheric wind speeds from unknown sources and application to the 2010 December 25 bolide. *Geophys J Int* 2013. <https://doi.org/10.1093/gji/ggt228>
- Borovicka J, Spurny P, Brown PG, Wiegert P, Kalenda P, Clark D, Shrubny L (2013) The trajectory, structure and origin of the Chelyabinsk asteroidal impactor. *Nature* 503:235–237. <https://doi.org/10.1038/nature12671>

- Brown PG, Whitaker RW, ReVelle DO (2002) Multi-station infrasonic observation of two large bolides: signal interpretation and implications for monitoring of atmospheric explosions. *Geophys Res Lett* 29. <https://doi.org/10.1029/2001gl013778>
- Brown PG et al (2013) A 500-kt airburst over Chelyabinsk and an enhanced hazard from small impactors. *Nature* 503:238–241. <https://doi.org/10.1038/nature12741>
- Cansi Y (1995) An automatic seismic event processing for detection and location: the PMCC method. *Geophys Res Lett* 22:1021–1024. <https://doi.org/10.1029/95GL00468>
- Ceranna L, Matoza R, Hupe P, Le Pichon A, Landès M (2019) Systematic array processing of a decade of global IMS infrasound data. In: Le Pichon A, Blanc E, Hauchecorne A (eds) *Infrasound monitoring for atmospheric studies*, 2nd edn. Springer, Dordrecht, pp 471–482
- De Groot-Hedlin C, Hedlin MAH (2014) Infrasound detection of the Chelyabinsk meteor at the USArray. *Earth Planet Sci Lett* 402:337–345. <https://doi.org/10.1016/j.epsl.2014.01.031>
- Drob DP, Picone JM, Garcés M (2003) Global morphology of infrasound propagation. *J Geophys Res* 108(D21):4680. <https://doi.org/10.1029/2002JD003307>
- Drob DP et al (2008) An empirical model of the Earth's horizontal wind fields: HWM07. *J Geophys Res* 113:A12304. <https://doi.org/10.1029/2008JA013668>
- Drob DP, Garcés M, Hedlin MAH, Brachet N (2010) The temporal morphology of infrasound propagation. *Pure Appl Geophys* 167:437–453. <https://doi.org/10.1007/s00024-010-0080-6>
- Edwards WN (2010) Meteor generated infrasound: theory and observation. *Infrasound monitoring for atmospheric studies*. Springer, Heidelberg, Germany, pp 361–414
- Ens TA, Brown PG, Edwards WN, Silber EA (2012) Infrasound production by bolides: a global statistical study. *J Atmos Sol Terr Phys* 80:208–229. <https://doi.org/10.1016/j.jastp.2012.01.018>
- Garcés M, Hansen RA, Lindquist KG (1998) Traveltimes for infrasonic waves propagating in a stratified atmosphere. *Geophys J Int* 135:255–263. <https://doi.org/10.1046/j.1365-246X.1998.00618.x>
- Heimann S, Gonzáles Á, Wang R, Cesca S, Dahm T (2013) Seismic characterization of the Chelyabinsk meteor's terminal explosion. *Seismol Res Lett* 84(6):1021–1025. <https://doi.org/10.1785/0220130042>
- Henneton M, Gainville O, Coulouvrat F (2015) Numerical simulation of sonic boom from hypersonic meteoroids. *AIAA J* 53(9):2560–2570. <https://doi.org/10.2514/1.J053421>
- Krasnov VM, Drobzheva YV, Salikhov NM, Zhumabaev BT, Lazurkina VB (2014) Estimation of the power of the Chelyabinsk meteorite blast from optical, seismic, and infrasonic observation data. *Acoust Phys* 60(2):155–162. <https://doi.org/10.1134/S1063771014020110>
- Le Pichon A, Vergoz J, Blanc E, Guilbert J, Ceranna L, Evers L, Brachet N (2009) Assessing the performance of the International Monitoring System's infrasound network: geographical coverage and temporal variabilities. *J Geophys Res* 114:D08112. <https://doi.org/10.1029/2008JD010907>
- Le Pichon A, Ceranna L, Vergoz J (2012) Incorporating numerical modeling into estimates of the detection capability of the IMS infrasound network. *J Geophys Res* 117:D05121. <https://doi.org/10.1029/2011JD016670>
- Le Pichon A, Ceranna L, Pilger C, Mialle P, Brown D, Herry P, Brachet N (2013) The 2013 Russian fireball largest ever detected by CTBTO infrasound sensors. *Geophys Res Lett* 40:3732–3737. <https://doi.org/10.1002/grl.50619>
- Le Pichon A, Ceranna L, Vergoz J, Tailpied D (2019) Modeling the detection capability of the global IMS infrasound network. In: Le Pichon A, Blanc E, Hauchecorne A (eds) *Infrasound monitoring for atmospheric studies*, 2nd edn. Springer, Dordrecht, pp 593–604
- Marty J (2019) The IMS infrasound network: current status and technological developments. In: Le Pichon A, Blanc E, Hauchecorne A (eds) *Infrasound monitoring for atmospheric studies*, 2nd edn. Springer, Dordrecht, pp 3–62
- Miller SD, Straka WC III, Bachmeier AS, Schmit TJ, Partain PT, Noh Y-J (2013) Earth-viewing satellite perspectives on the Chelyabinsk meteor event. *Proc Natl Acad Sci USA* 110:18092–18097. <https://doi.org/10.1073/pnas.1307965110>

- Picone JM, Hedin AE, Drob DP, Aikin AC (2002) NRLMSISE-00 empirical model of the atmosphere: statistical comparisons and scientific issues. *J Geophys Res* 107:1468–1483. <https://doi.org/10.1029/2002JA009430>
- Pilger C, Streicher F, Ceranna L, Koch K (2013) Application of propagation modeling to verify and discriminate ground-truth infrasound signals at regional distances. *Inframatrics* 2013 2:39–55. <https://doi.org/10.4236/inframatrics.2013.24004>
- Pilger C, Ceranna L, Ross JO, Le Pichon A, Mialle P, Garcés M (2015) CTBT infrasound network performance to detect the 2013 Russian fireball event. *Geophys Res Lett* 42. <https://doi.org/10.1002/2015gl063482>
- Popova OP et al (2013) Chelyabinsk airburst, damage assessment, meteorite recovery, and characterization. *Science* 342:1069–1073. <https://doi.org/10.1126/science.1242642>
- ReVelle DO (1997) Historical detection of atmospheric impacts by large bolides using acoustic-gravity waves. *Ann N Y Acad Sci* 822:284–305. <https://doi.org/10.1111/j.1749-6632.1997.tb48347.x>
- ReVelle DO, Brown PG, Spurny P (2004) Entry dynamics and acoustic/infrasonic/seismic analysis for the Neuschwanstein meteorite fall. *Meteorit Planet Sci* 39(10):1605–1626. <https://doi.org/10.1111/j.1945-5100.2004.tb00061.x>
- Silber EA, Le Pichon A, Brown PG (2011) Infrasonic detection of a near-earth object impact over Indonesia on 8 October 2009. *Geophys Res Lett* 38:L12201. <https://doi.org/10.1029/2011GL047633>
- Silber EA, Brown PG (2014) Optical observations of meteors generating infrasound-I: acoustical signal identification and phenomenology. *J Atmos Sol Terr Phys* 119:116–128. <https://doi.org/10.1016/j.jastp.2014.07.005>
- Silber EA, Brown PG (2017) Infrasound monitoring to identify potentially dangerous NEO. In: Le Pichon A et al (eds) *Infrasound monitoring (Challenges and new perspective)*. Springer
- Silber E, Brown P (2019) Infrasound monitoring as a tool to characterize impacting near-earth objects (NEOs). In: Le Pichon A, Blanc E, Hauchecorne A (eds) *Infrasound monitoring for atmospheric studies*, 2nd edn. Springer, Dordrecht, pp 939–986
- Tauzin B, Debayle E, Quantin C, Coltice N (2013) Seismoacoustic coupling induced by the breakup of the 15 February 2013 Chelyabinsk meteor. *Geophys Res Lett* 40:3522–3526. <https://doi.org/10.1002/grl.50683>
- Whipple FJW (1930) The great Siberian meteor and the waves, seismic and aerial, which it produced. *Quart J R Meteorol Soc* 56:287–304. <https://doi.org/10.1002/qj.49705623601>